Structural Chemistry
https://doi.org/10.1007/s11224-025-02600-9

RESEARCH

Synthesis, characterization, chemical reactivity, optical, and biological investigations of (E)-1-phenyl-3-(p-tolyl)prop-2-en-1-one

Mohamed Ibrahim Sulaiman Sait Shahul Hameed[1] · Raj Muhamed Rahiman Sahib[1] · Kumaran Subramanian[2] · Muzammil Pookutti[3] · Thirunavukkarasu Manickavelu[4] · Naveen Kosar[5] · Rajesh Punniyamoorthy[6] · Chakkaravarthy Perumal[7] · Dhanalakshmi Karuppaiyan[8] · Raja Murugesan[9]

Received: 4 July 2025 / Accepted: 17 August 2025

Abstract

The chalcone derivatives, commonly found in plant-derived compounds, are widely used in pharmaceutical and optical activities. In this study, the (E)-1-phenyl-3-(p-tolyl)prop-2-en-1-one (1P3P2O) molecule is synthesized and characterized by experimental and theoretical spectroscopic (FT-IR, UV–Vis, and NMR) techniques. The theoretical calculations of the 1P3P2O molecule are calculated using Density Functional Theory (DFT) with the B3LYP/6–311 + + G(d,p) basis set. The research explores molecular vibrational modes, chemical characteristics, and electronic behavior, including potential energy surfaces, geometry optimization, and vibrational frequencies. Theoretical findings are compared to experimental data, especially concerning the compound's chemical properties. The study also investigated frontier molecular orbitals (FMO) and electron–hole excitations across a range of solvents, including DMSO, chloroform, water, and methanol. Furthermore, the analysis of natural bond orbitals (NBO), molecular electrostatic potential (MEP), and Fukui functions (f +, f-, f0) enhanced the understanding of the electronic structure. The optical activity of the title molecule is investigated through nonlinear optical (NLO) parameters. Molecular docking simulations using AutoDock software demonstrated substantial binding interactions between the 1P3P2O compound and an antiviral protein, with a binding energy of − 7.56 kcal/mol.

Keywords Spectroscopic · NMR · Chemical reactivity · NLO activity · Topology · Molecular docking

✉ Raj Muhamed Rahiman Sahib
ponnu_68@yahoo.co.in

✉ Chakkaravarthy Perumal
p.chakku76@gmail.com

✉ Raja Murugesan
raja.physics2014@gmail.com

[1] Department of Physics, Jamal Mohamed College (Autonomous) (Affiliated to Bharathidasan University), Tiruchirappalli 620020, Tamil Nadu, India

[2] Department of ECE, Saveetha School of Engineering, Saveetha Institute of Technical and Medical Sciences(SIMATS), Thandalam, Chennai, 602105, Tamil Nadu, India

[3] Department of Physics, Islamiah College (Autonomous), Vaniyambadi, Tirupattur, Tamil Nadu 635752, India

[4] Department of Physics, Vel Tech Rangarajan Dr. Sagunthala R&D Institute of Science and Technology, Avadi, Chennai 600062, India

[5] Department of Chemistry, University of Management and Technology (UMT), C-11, Johar Town, Lahore, Pakistan

[6] Department of Physics, School of Basic Science, Vels Institute of Science and Technology & Advanced Studies, Pallavaram, Chennai 600 117, Tamil Nadu, India

[7] Department of Chemistry, Thirumagal Mill's College, Gudiyattam, Govt 632602, Tamil Nadu, India

[8] Department of Physics, Periyar Maniammai Institute of Science & Technology, Vallam, Thanjavur 613403, Tamil Nadu, India

[9] Department of Physics, Govt. Thirumagal Mill's College, Gudiyattam 632602, Tamil Nadu, India

Published online: 07 September 2025

Introduction

Natural sources continue to be a primary source of inspiration for the development of novel chemical entities with promising optical and medicinal properties. This research focuses on the chalcone derivative (E)−1-phenyl-3-(p-tolyl)prop-2-en-1-one, which features a ketone functional group and a three-carbon side chain. The compound's specific "(E)" configuration, which denotes the unique orientation of the phenyl and p-tolyl groups around the conjugated double bond, has drawn attention due to its potential pharmacological implications, particularly in the field of antiviral activity. To gain an expanded understanding of the compound, a thorough review of recent literature is essential.

Chalcones, belonging to the flavonoid family, are widely recognized for their characteristic α,β-unsaturated carbonyl group, which is common in many plant species. The stability and low redox potential of chalcones arise from the extended conjugation between the electrophilic α,β-unsaturated carbonyl center and the aromatic rings. These compounds exhibit diverse pharmacological activities, including anti-inflammatory, antiprotozoal, antiviral, anti-leishmanial, antidepressant, anticancer, antimalarial, anticonvulsant, anti-diabetic, and antioxidant. This broad spectrum of biological activities makes chalcones highly relevant to medicinal chemistry, emphasizing the need for further theoretical and experimental investigation.

Recent research has explored a variety of chalcone derivatives. Takaki and Ashburn (2022) analyzed "(E)−3-[4-(1H-Imidazol-1-yl)phenyl]−1-(3-chloro-4-fluorophenyl)prop-2-en-1-one," shedding light on its distinctive molecular features [1]. Similarly, Bailey and Ashburn (2021) focused on "(E)−3-[4-(1H-Imidazol-1-yl) phenyl]−1-(4-methylphenyl)prop-2-en-1-one," offering insights into its molecular structure [2]. Koh (2022) provided a crystallographic study of "(E)−1-(2-Hydroxy-4,6-dimethoxyphenyl)−3-(naphthalen-1-yl)prop-2-en-1-one," advancing the understanding of its crystal lattice [3]. Rasool et al. (2022) examined two chalcone derivatives, "(E)−3-(4-ethoxyphenyl)−1-(2-(trifluoromethyl)phenyl) prop-2-en-1-one" and "(E)−3-(naphthalen-2-yl)−1-(2-(trifluoromethyl)phenyl)prop-2-en-1-one," investigating their potential applications in DNA binding, urease inhibition, and nonlinear optical behavior [4]. Aldaghri (2021) contributed to the literature by analyzing the spectral and molecular characteristics of "(E)−1-(4-chlorophenyl)−3-(4-(dimethylamino)phenyl)prop-2-en-1-one" in Materials [5]. Zou et al. (2018) discussed the synthesis and optimization of "(E)−3-(dimethylamino)−1-(1H-indol-3-yl)prop-2-en-1-one" [6], while Sadgir et al. (2020) synthesized and characterized "(2E)−3-(2,6-dichlorophenyl)−1-(4-methoxyphenyl)-prop-2-en-1-one," offering valuable X-ray diffraction, DFT, and antimicrobial data in SN Applied Sciences [7]. Finally, Borul and Agarkar (2020) explored the synthesis and drug-likeness of "(E)−3-substituted phenyl-1-piperidino-2-propen-1-one cinnamamide," evaluating its pharmaceutical potential [8].

Due to its great accuracy in predicting molecular properties, researchers have been adopting quantum chemical calculations progressively in recent years. One such common approach is Density Functional Theory (DFT) with the 6–311 + + G(d,p) basis set [9–13]. The present study is the detailed spectroscopic analysis of the (E)−1-phenyl-3-(p-tolyl)prop-2-en-1-one (1P3P2O) molecule. Additionally, DFT calculations are performed, incorporating Frontier Molecular Orbital (FMO) and Natural Bond Orbital (NBO) analysis for elucidating the electronic characteristics. Intramolecular interactions of the 1P3P2O molecule are performed by the Hirshfeld surface analysis. Furthermore, the in silico antiviral potential of the 1P3P2O molecule is evaluated through molecular docking simulations. This research aims to provide critical perceptions of the composite's properties and its potent applications in antiviral drug development.

Materials and methods

Synthesis of (E)−1-phenyl-3-(p-tolyl) prop-2-en-1-one (1P3P2O)

The synthesis of (E)−1-phenyl-3-(p-tolyl)prop-2-en-1-one (1P3P2O) was initiated by dissolving 0.01 mol of acetophenone and 0.01 mol of 4-methylbenzaldehyde in 100 mL of ethanol. To this solution, 20 mL of a 10% potassium hydroxide (KOH) solution (0.02 mol) was added dropwise while stirring the mixture at room temperature for 12 h. Following this, the mixture was poured onto crushed ice and acidified with dilute HCl in a 1:1 ratio. The resultant was separated by filtration. The crude product was then cleansed via recrystallization by means of acetic acid. The result in compound's purity has been confirmed using thin-layer chromatography (TLC). The synthesis procedure is represented in Fig. 1.

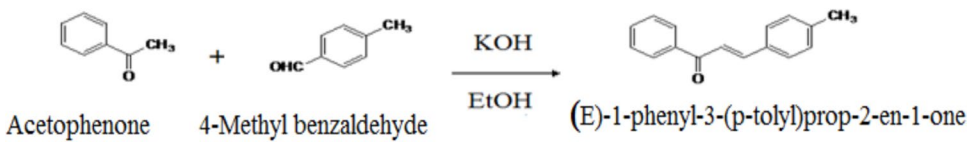

Fig. 1 The synthesis of (E)−1-phenyl-3-(p-tolyl)prop-2-en-1-one

Instrumentation details

FT-IR spectroscopy was performed at 4000–400 cm^{-1} for the title compound. Bruker instruments were utilized to collect 1H and 13C NMR spectra at 400 MHz. FT-IR and NMR spectra were acquired at the Science Instrumentation Facility (SIF) at VIT University in Vellore, India.

Computational methods

The molecular system was extensively analyzed using Gaussian 09W software, applying the B3LYP/6-311G + + (d,p) level of theory [14]. This approach involved optimizing the molecular geometry to determine the most stable conformation, followed by a detailed investigation of its vibrational characteristics and chemical properties. GaussView was employed to visualize the molecular structure. In addition to these structural and vibrational studies, theoretical NMR spectra were also computed. To further understand the electron distribution, a topological analysis was performed using the Multiwfn software [15]. The UV–visible spectrum was calculated with TD-DFT, taking into account solvation effects. Finally, the AutoDock [16] software was employed to explore the molecular biological potential of the 1P3P2O molecule.

Results and discussion

Geometrical optimization and stable conformations

The stable conformation of the 1P3P2O molecule is investigated by potential energy scan (PES) analyses. The two torsion angles (SC1 = O4-C1-C5-C10, SC2 = O4-C1-C2-C3) are rotated 360 degrees (10 steps, and each step is rotated 36 degrees). The most stable energy of 1P3P2O is obtained at − 0.033693 Hartree for torsion angles SC1 at − 43.37661° and SC2 at − 0.100330°, as shown in Figs. 2 and 3. The optimal structural parameters of the 1P3P2O molecule are summarized in Table S1. The 1P3P2O molecule has 17 C–C bond lengths, 14 C-H bond lengths, and one O-C bond length. M. Edward et al. [17] provided the experimental X-ray diffraction (XRD) data for this molecule. A comparison of experimental and computational results (exp./cal.) demonstrates strong agreement, particularly for key bond lengths such as the C1-C2 single bond (1.474/1.486 Å), C1 = O4 double bond (1.224/1.227 Å), and C2 = C3 double bond (1.326/1.346 Å). In the solid state, the molecular packing is dominated by weak C-H–-O and C-H–-π interactions, as shown in Fig. 3. These interactions, with distances greater than 2.54 Å, highlight the consistency between the gas-phase computational results and the experimental solid-state structure. It should be noted that Gaussian calculations are more suited to isolated molecules in the gas phase. Furthermore, bond angles such as C2-C1-O4, C6-C7-C8, and C6-C7-H21 show excellent correlation between observed and calculated parameters, further supporting the accuracy of the computational model, as listed in Table S1.

Spectral analysis

A detailed spectral analysis was conducted to elucidate the functional groups within the 1P3P2O molecule. With a molecular structure comprising 31 atoms, 1P3P2O exhibits 87 significant vibrational modes. The calculated unscaled vibrational frequencies are scaled using a scaling factor of 0.961 [18]. The potential energy distribution (PED) analysis has been employed to assign the vibrational modes [19]. Table S2 presents a thorough overview of the theoretical and experimental frequencies, together with their assignments, and Fig. S1 shows graphical comparisons of the experimental and theoretical FT-IR spectra.

CH and CH3 vibrations

The C-H stretching vibrations of aromatic compounds usually exhibit in the region 3100–3000 cm^{-1} [20, 21]. However, interpreting the C-H vibrations in the IR spectra can be complex due to the influence of different substituents and their arrangements. In this study, C-H stretching vibrations (Mode nos: 1–10) were identified at various frequencies. The experimental FT-IR spectrum exhibited peaks at 3240 and 3034 cm^{-1}, while the theoretical predictions were at 3042, 3036, 3033, 3017, 3015, 3004, 2999, 2993, 2992, and 2986 cm^{-1}. The PED analysis indicated that the stretching C-H modes of 1P3P2O are primarily pure, with contributions close to 100%.

The 1P3P2O molecule contains a CH3 group, which contributes 12 normal modes of vibration such as three bending modes, two asymmetric stretching modes (asymd), two symmetric stretching modes (symd), two rocking modes, and one torsional mode among the nine modes that characterize the vibrations within the CH3 group. The C-CH3 bonds' bending and stretching vibrations are described by each of the remaining modes. Generally, the CH3 asymmetrical stretching presented at 2980 cm^{-1} region with symmetric stretching near the same region [22, 23]. Due to the asymmetric CH3 stretching vibrations, FT-IR spectra exhibit peaks at 2968 and 2927 cm^{-1}, and the theoretically calculated values are at 2928 and 2907 cm^{-1} (mode numbers 11 and 12). The CH3 symmetric stretching vibration is computed at 2860 cm^{-1} (mode number 13). Deformation modes of the CH3 group in methyl-substituted benzene derivatives are typically found between 1465–1440 cm^{-1} (asymmetric) and 1390–1370 cm^{-1} (symmetric) [24]. For this molecule, the asymmetric deformation vibrations

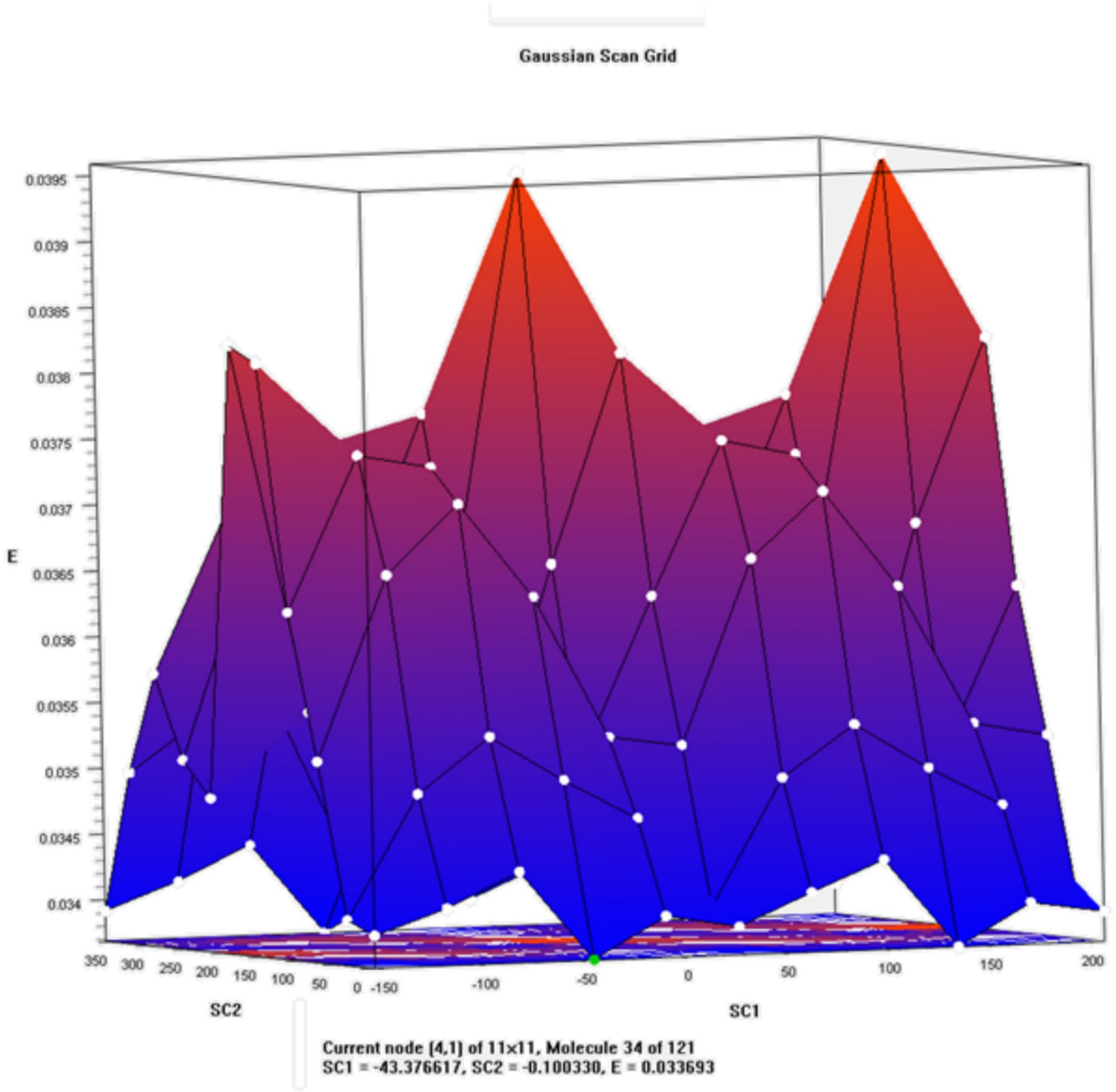

Fig. 2 Potential energy surface scan of 1P3P2O

occur between 1415 and 1406 cm^{-1} (mode numbers 23 and 24). The symmetric deformation vibration is calculated at 1318 cm^{-1} (mode number 27), which is in excellent accordance with the recorded value of 1317 cm^{-1}. Additionally, the CH3 group undergoes rocking vibrations, typically in the 1070–1010 cm^{-1} range [25]. The CH3 rocking mode calculated at 1002 cm^{-1} (mode number 43) matches well with values reported in the literature. The CH3 torsional vibration, which occurs at low wavenumbers, is predicted at 165 cm^{-1} (mode number 79), consistent with expected values for CH3 torsion.

C–C stretching vibrations

In general, the C–C stretching vibrations occur in the region 1625–1430 cm^{-1} [26, 27]. The experimental FT-IR spectrum of 1P3P2O molecule is noted at 1643, 1427 cm^{-1} and calculated at 1646, 1557, 1548, 1526, 1514, 1393, and 1364 cm^{-1} are clearly assigned to the aromatic C–C stretching vibrations.

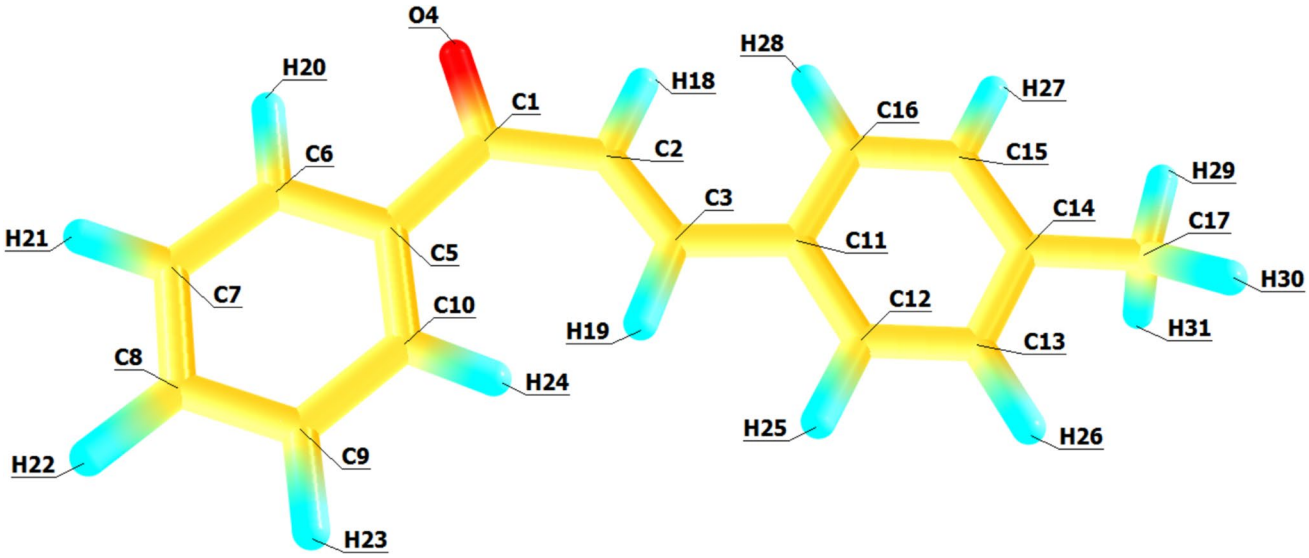

Fig. 3 Optimized geometric structure of 1P3P2O

C = O vibrations

The C = O carbonyl bond is formed by the overlap of pi-orbitals between the carbon (C) and oxygen (O) atoms. Usually, the C = O bond appears in the 1800–1500 region [28, 29]. In this study, the C = O stretching vibration was recorded at 1597 cm^{-1} and theoretically computed at 1598 cm^{-1} in the FT-IR spectrum. Additionally, the in-plane deformation of the CCO bond is predicted at 711 and 548 cm^{-1}, while the out-of-plane deformation is calculated at 642 cm^{-1}. The theoretical and recorded correlation graph ($R^2 = 0.999$) of the 1P3P2O molecule is shown in Fig. S2.

NMR spectral analysis

The nuclear magnetic resonance (NMR) is attracting much attention for organic molecules to identify the carbon and hydrogen atoms. In the present study, the ^{13}C and ^{1}H NMR spectra of synthesized 1P3P2O molecule are recorded and calculated using DMSO solvent. The ^{13}C and ^{1}H NMR chemical shifting values of 1P3P2O molecule are tabulated in Table S3, and spectra are displayed in Figs. S3 and S4. Theoretical chemical shifts are calculated using the B3LYP method with the GIAO approach, showing strong consistency with the experimental ^{13}C NMR data. In general, the 13 C NMR chemical shifts are observed at above 100 ppm [30].

The highest chemical shift is found at C1 (197.3(exp)/197.4 ppm (theo)), influenced by the electronegative oxygen atom of O4, while the methyl group carbon (C17) shows a shift at 43.82/43.91 ppm. The carbonyl carbon (C1) shows excellent consistency, with measured and calculated values of 197.34 and 197.45 ppm, respectively. Alkene carbons C2 and C3 appear at 136.53(exp)/137.75 ppm (theo) and 189.16(exp)/182.01 ppm (theo). Aromatic carbons C5–C16 mostly fall between 128 and 140 ppm, with minimal deviations. The para substituted aromatic carbon (C14) is more downfield at 154.36 ppm(exe)/157.92 ppm(theo), while the methyl carbon (C17) appears at 44.82 ppm (exe)/43.91 ppm (theo).

The H18–H20 protons observed at 7.8–8.0 ppm and calculated at 8.78–8.99 ppm. Aromatic protons H21–H28 generally differ by less than 0.3 ppm, except H28, which shows a larger offset of about 1.8 ppm. The p-tolyl methyl protons (H29) are closely matched at 2.39 vs. 2.45 ppm, and alkyl protons H30 and H31 appear at roughly 1.675 ppm in both cases. Overall, the computational method reproduces ^{13}C shifts with high precision (within 0.1–2 ppm).

Electronic properties: UV–visible spectral analysis

UV–Vis spectroscopy carefully examined the electronic properties of 1P3P2O to explore its electronic transitions. The UV–Vis spectrum was recorded in DMSO solvent and computed in gas phase and solvent phase (DMSO, ethanol). The absorption wavelengths, energies, oscillator strengths, and band gap values are calculated using the time-dependent Density Functional Theory (TD-DFT) [31] and the data are tabulated in Table 1. The comparison of experimental and theoretical absorption spectra of the 1P3P2O molecule is obtained in Fig. S5. The absorption maximum of 1P3P2O molecule is recorded for DMSO solvent was found at 316 nm, and the theoretically calculated values are 324 nm (gas), 343 nm (DMSO), and 342 nm (ethanol), while band gap energies were recorded at 3.9339 eV (DMSO) and theoretically obtained values are 3.8378 eV (gas), 3.6204 eV

Table 1 Experimental computed electronic transition states of 1P3P2O with TD-DFT method

Solvent	Experimental	Band gap (eV)	Energy (cm^{-1})	Wave-length (nm)	Band gap(ev)V	Osc. Strength	Major contribs
Gas			26,033	384	3.2362	0.0067	H-1->LUMO (90%)
			30,872	324	3.8378	0.7062	HOMO->LUMO (95%)
			34,708	288	4.3145	0.0106	H-3->LUMO (13%), H-2->LUMO (81%)
DMSO			27,470	364	3.4148	0.0648	H-4->LUMO (13%), H-1->LUMO (72%)
	316	3.9339	29,124	343	3.6204	0.7616	HOMO->LUMO (89%)
			33,550	298	4.1707	0.0151	H-2->LUMO (92%)
Ethanol			27,433	365	3.4102	0.0543	H-4->LUMO (13%), H-1->LUMO (74%)
			29,226	342	3.6331	0.7615	HOMO->LUMO (90%)
			33,603	298	4.1772	0.0147	H-2->LUMO (92%)

(DMSO), and 3.6331 eV (ethanol). The HOMO–LUMO electronic transitions are observed for the 1P3P2O molecule at 95% in the gas phase, 89% in DMSO, and 90% in ethanol solvent, and $\pi \rightarrow \pi^*$ transitions are observed for the present investigations.

Frontier molecular orbital (FMO) analysis

The FMO analysis plays a vital role in understanding the chemical stability and reactivities of organic molecules [32–37]. Here, the molecular orbitals of the title compound were examined in three different environments: gas phase, DMSO, and ethanol solvents. The HOMO–LUMO energy transition of the 1P3P2O compound is exhibited in Fig. 4. The band gap energy and their parameters of the HOMO and the LUMO were calculated and reported in Table 2. Table 2 shows the following results:

Gas phase: HOMO = − 6.4769 eV, LUMO = − 2.3407 eV, band gap = 4.1362 eV.

DMSO: HOMO = − 6.5351 eV, LUMO = − 2.5222 eV, band gap = 4.0129 eV.

Ethanol: HOMO = − 6.5319 eV, LUMO = − 2.5149 eV, band gap = 4.0170 eV.

The small variations in the band gap across these different solvents suggest that 1P3P2O exhibits consistent electronic properties of the surrounding medium. These low band gap values suggest that it may possess bioactive properties.

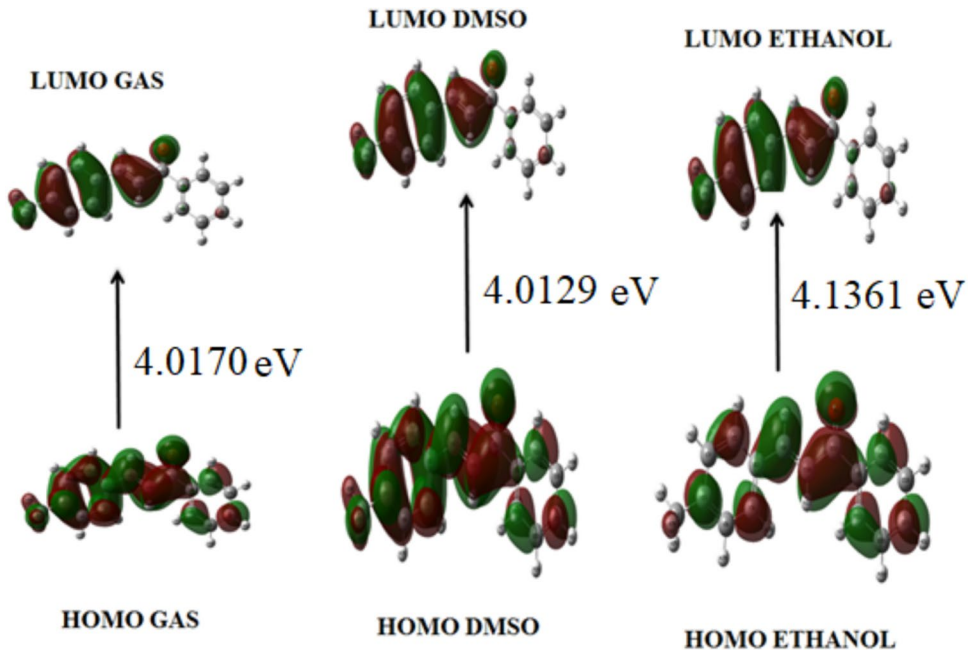

Fig. 4 HOMO–LUMO diagram of title molecule using gas, DMSO, and ethanol solvents

Table 2 Calculated energy values at various solvents

Properties	Solvents		
	Ethanol	**DMSO**	**Gas**
HOMO (eV)	−6.5319	−6.5351	−6.4769
LUMO (eV)	−2.5149	−2.5222	−2.3407
Ionization potential	6.5319	6.5351	6.4769
Electron affinity	2.5149	2.5222	2.3407
Energy gap (eV)	4.0170	4.0129	4.1362
Electronegativity	4.5234	4.5287	4.4088
Chemical potential	−4.5234	−4.5287	−4.4088
Chemical hardness	2.0085	2.0065	2.0681
Chemical softness	0.2489	0.2492	0.2418
Electrophilicity index	5.0936	5.1107	4.6994

Molecular electrostatic potential (MEP) analysis

Molecular electrostatic potential (MEP) is an important parameter for investigating molecular electrostatic properties and identifying reactive regions that may interact with between bonds [38–41]. In the present study, the MEP map of 1P3P2O molecule is elucidated different environment in gas and liquid phases (DMSO and ethanol) as shown in Fig. 5. The molecular reactivity's are identified for color grading technique such as red color indicating the negative potential and blue color indicating the positive potential. The oxygen atom (O4) in the molecule has a highly negative electrostatic potential, shown in red on the MEP. This suggests that O4 is likely to interact with positively charged regions, such as hydrogen atoms in amino acids, of its electron-rich nature. The region around the O4-C1 bond exhibits a positive charge (blue), indicating an electropositive area that could interact with electron-donating species. Furthermore, molecular electrostatic potential is observed between ranges from -5.771×10^{-2} to 5.771×10^{-2} a.u (gas), -7.094×10^{-2} to 7.094×10^{-2} a.u (DMSO) and -7.050×10^{-2} to 7.050×10^{-2} a.u (ethanol). These values are clearly indicated that the DMSO solvent is more reactive compare to gas and ethanol solvent.

Fukui function analysis

The Fukui function describes the chemical reactivity of individual atoms within a molecule in relation to electrophilic and nucleophilic attacks [42, 43]. In this study, the Fukui function and dual descriptors are calculated using Mulliken population analysis (MPA) [44] as shown in Table S4. The

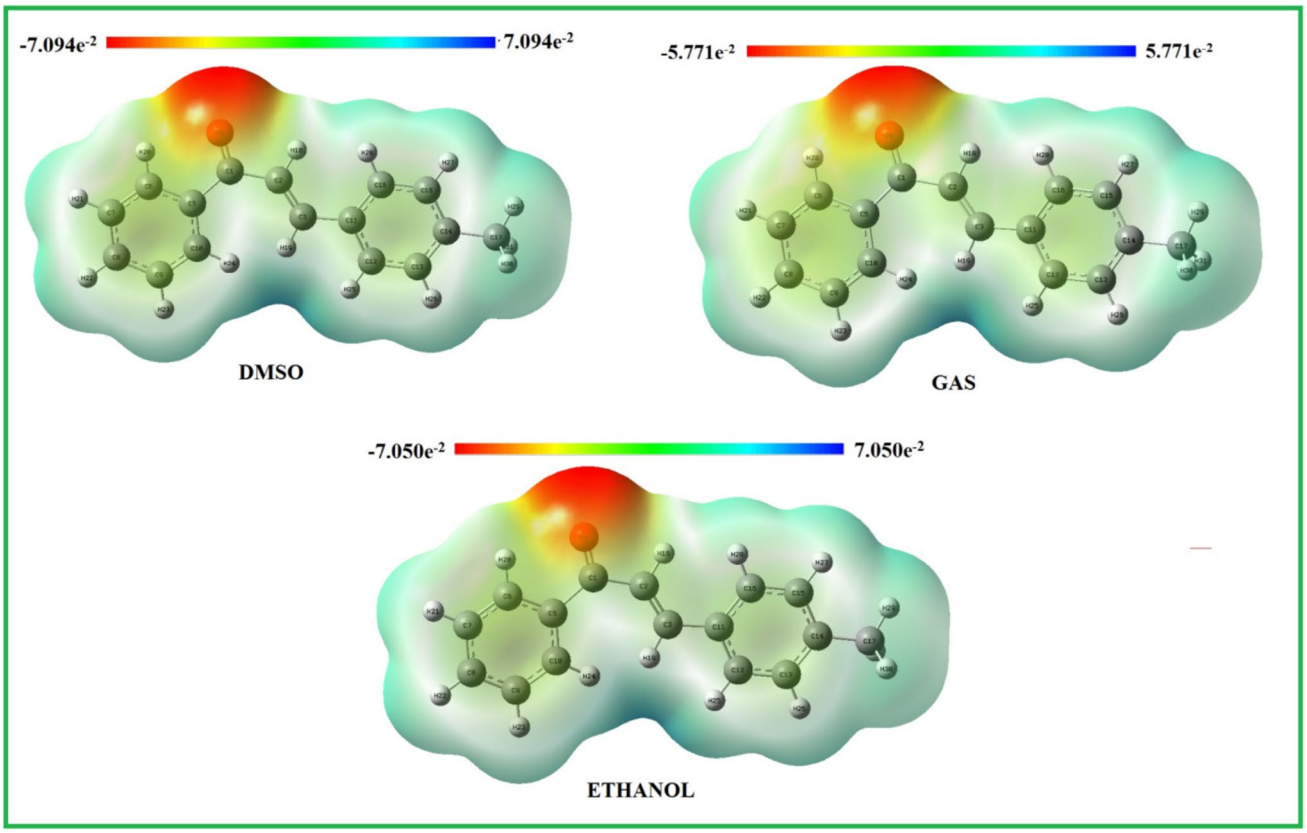

Fig. 5 MEP map of 1P3P2O molecule using different solvents (gas, DMSO, and ethanol)

dual descriptors are very useful to simply understand the chemical reactivities; the positive values indicate nucleophilic attack, while a negative value suggests a region that is more likely to undergo electrophilic attack. Table S4 shows the electrophilic regions: C7 (−0.0273), C11 (−0.0347), and C14 (−0.0360) atoms exhibit higher susceptibility to nucleophilic attacks, and the nucleophilic regions: C1 (0.0638), O4 (0.0293), and C8 (0.0360) atoms are more prone to electrophilic attack. These results indicate that 1P3P2O is more likely to undergo nucleophilic attack at positions C7, C11, and C14, while positions C1, O4, and C8 are more reactive to electrophilic attack. This data has significance for forecasting how 1P3P2O would behave chemically through various reactions.

Charge-transfer and electron–hole dynamics

Electron–hole analyses are utilized to determine electron distributions in organic compounds [45]. The charge transfer of 1P3P2O is characterized by three excited states in three distinct solvents, as illustrated in Table 3, while Fig. 6 depicts the electron (green) and hole (blue) distributions throughout these transitions. In particular, the three excited states in all solvents have the following properties: D-index values suggesting significant hole-electron interactions. R-index values indicate a large geographic difference between the electron and hole centroids. T-index values indicate significant charge transfer (CT) excitation. The least excitation energy is observed in DMSO solvent (3.406(I), 3.611(II), 4.160(III)) compared to gas and ethanol solvent.

Electron density analysis: LOL and ELF

In this research study, two extensive computational techniques were used to conduct a thorough investigation in order to obtain a better understanding of the electron density distribution within the 1P3P2O molecule: Electron Localization Function (ELF) [46] and Localization Orbital Locator (LOL) [47]. These analyses were accomplished with the Multiwfn 3.8 analyzer, utilizing the data extracted from the Gaussian file (.fchk) output. The resulting ELF and LOL maps, shown in Figs. 7 and 8, display color-coded gradients to represent electron density: magenta signifies regions of high electron concentration, while red specifies lower concentration. Hydrogen atoms in magenta reflect high electron localization typical of non-bonding regions. Carbon and oxygen atoms are highlighted with blue and green circles, showing their electron density delocalization, which suggests bonding interactions. Magenta and blue regions surrounding carbon, chlorine, and nitrogen atoms indicate strong electron localization, which correlates with the concentration of electron density in their respective orbitals. This information is invaluable for understanding the compound's chemical behavior, potential reactivity, and interactions with other molecules, offering significant insights into its stability and bioactivity.

Nonlinear optical effects

Nonlinear optical (NLO) properties are of significant importance in modern technology, particularly in laser applications and related fields [48–51]. The NLO characteristics of 1P3P2O were investigated in solvents, including the gas phase, DMSO, and ethanol. The computed values for key NLO parameters are presented in Table 4. In the gas phase, the calculated values for 1P3P2O are: dipole moment 1.8999 D, polarizability 8.00267×10^{-23} esu, and first-order hyperpolarizability 19.500×10^{-30} esu. In DMSO, the values are: dipole moment 1.74693 D, polarizability 1.01915×10^{-23} esu, and first-order hyperpolarizability 4.0573×10^{-30} esu. In ethanol, the values are: dipole moment 2.1190 D, polarizability 1.1921×10^{-23} esu, and first-order hyperpolarizability 5.9893×10^{-30} esu. When these values are compared to the typical threshold values used for NLO materials, such as urea, which has a first-order hyperpolarizability of 0.372×10^{-30} esu, the first-order hyperpolarizability of 1P3P2O is approximately nine times superior, demonstrating

Table 3 Charge transfer and electron–hole

Parameter	DMSO			Ethanol			Gas		
	I	**II**	**III**	**I**	**II**	**III**	**I**	**II**	**III**
Excitation energy	3.406	3.611	4.160	3.228	3.828	4.303	3.412	3.803	4.311
H index	2.558	3.011	2.637	2.339	2.890	2.490	2.339	2.991	2.556
D index	1.393	2.029	3.481	1.875	2.147	3.868	1.576	2.165	3.490
Δr index	2.1928	2.4742	3.5226	2.0356	2.1469	3.4993	1.9885	2.5141	3.5713
t index	−0.452	−0.595	1.380	0.177	−0.360	2.004	−0.113	−0.424	1.457
sm index	0.2467	0.4031	0.2135	0.2012	0.4096	0.1215	0.2187	0.3973	0.2139
sr index	0.5035	0.6877	0.5229	0.4370	0.6785	0.3560	0.4687	0.6875	0.5276
Coulomb attraction energy	5.3568	4.9270	4.1003	4.9126	4.6128	3.7111	5.5747	4.7888	4.2466

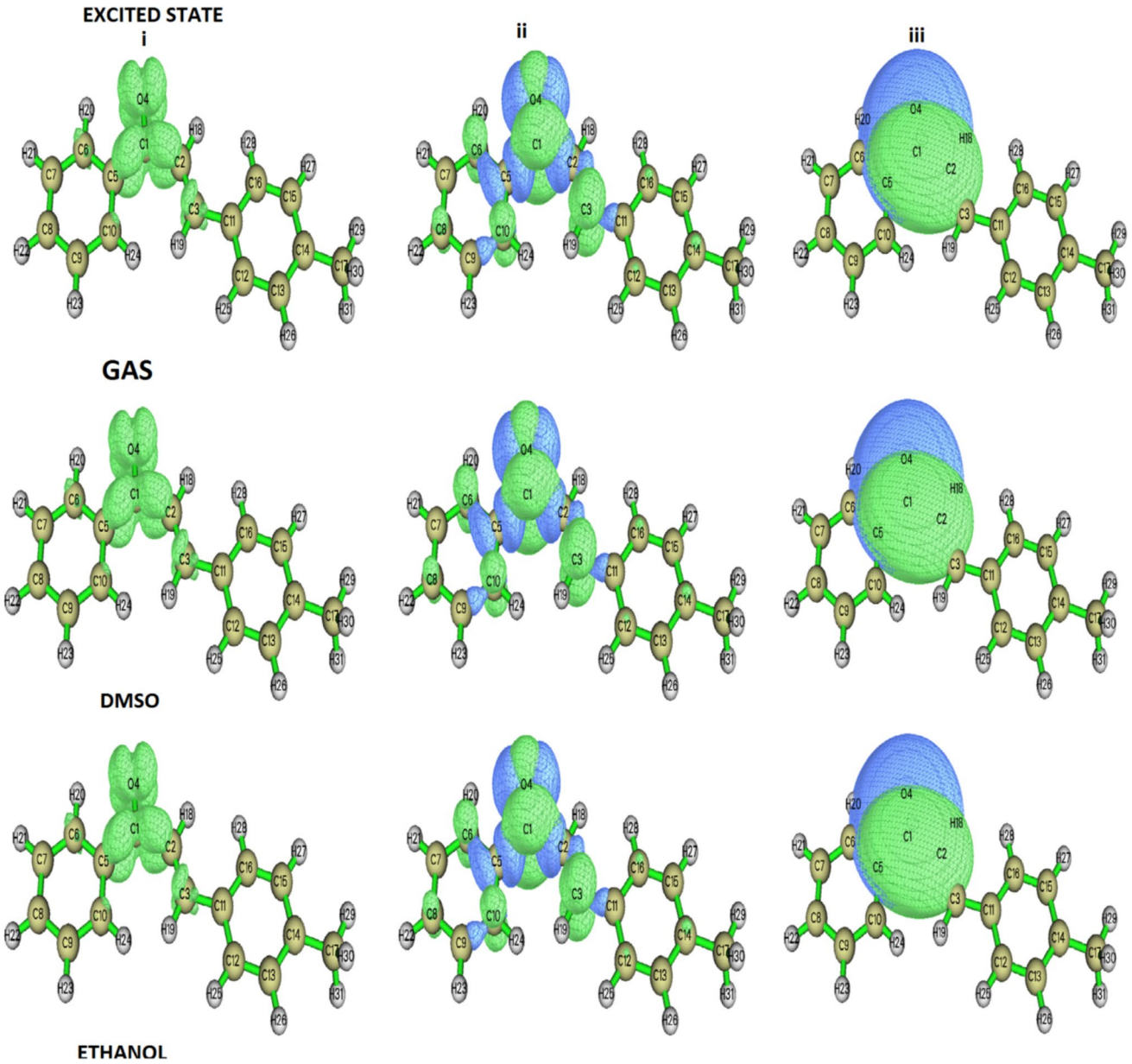

Fig. 6 Electron (green)-Hole (blue) distribution analysis for the GAS, DMSO, and ethanol solvents for the title compound

its significant NLO potential and making it a promising candidate for use in future NLO technologies.

NBO analysis

The NBO analysis of 1P3P2O was conducted using Gaussian 09 in conjunction with NBO 3.1, employing DFT/B3LYP methods [52]. The focus was on understanding secondary interactions within the molecule, and molecular interactions (donor–acceptor) were assessed using the second-order Fock-matrix approach [53, 54]. The significant hyper-conjugative intramolecular interactions are observed at the C–C bond, and the anti-bonding in the ring structure is shown in Table 5. Furthermore, extensive delocalization of π-electrons was observed in the C11-C12 bond, extending to the anti-bonding orbitals π*(C2-C3), π*(C13-C14), and π*(C15-C16). These delocalizations resulted in stabilization energies of 23.48, 20.14, and 21.03 kJ/mol, respectively. Additionally, the sigma system also exhibited significant donor–acceptor interactions. For instance, [C2-C3] → (C1-C2), (C3-C11), (C11-C12), and [C11-C12] → (C3-C11), (C11-C16), (C12-C13) interactions, as detailed in Table 5, contributed to the overall electronic structure. The lone pair LP(2)O4 participated in interactions with σ*(C1-C2) and

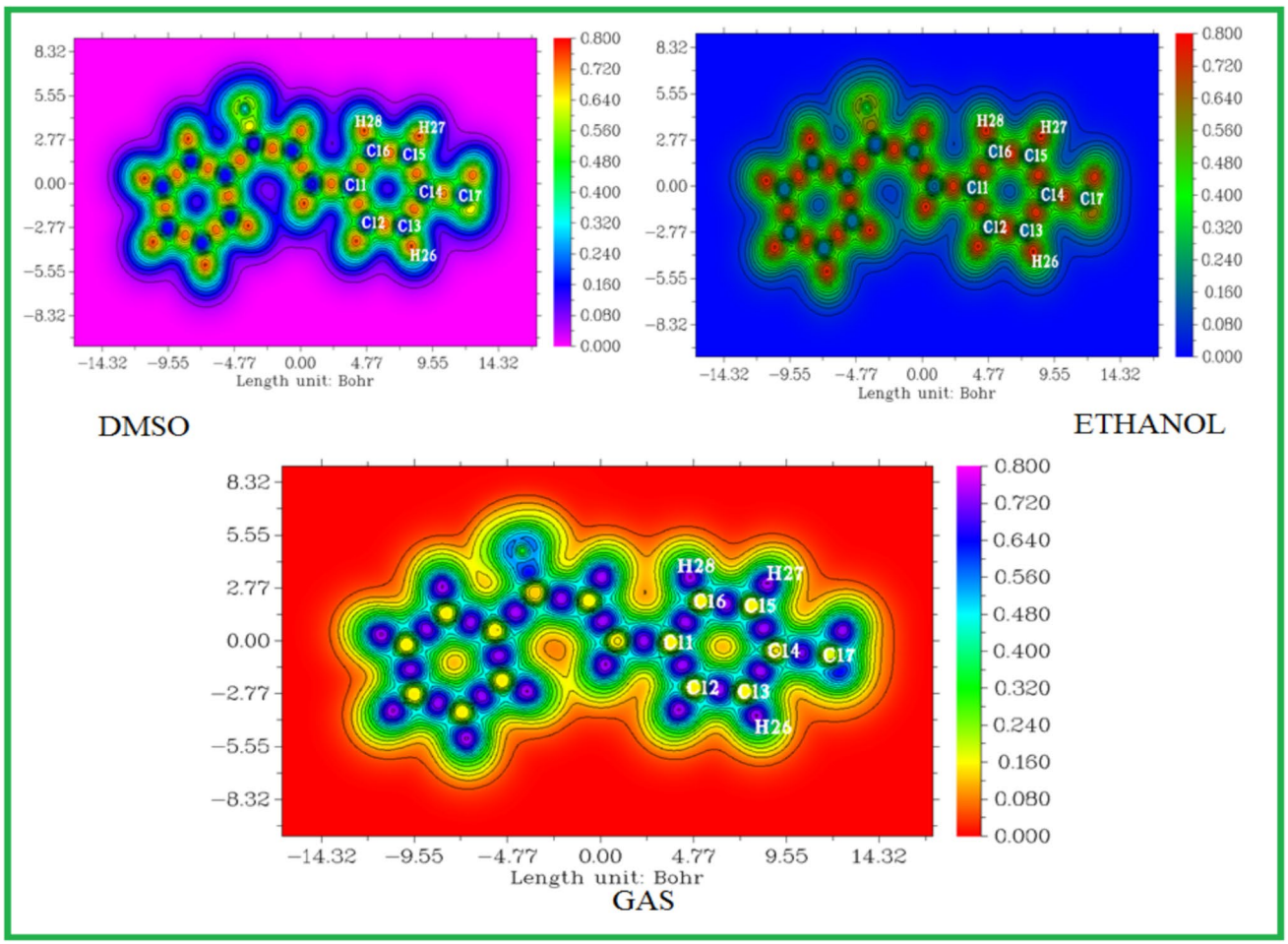

Fig. 7 ELF plot of title molecule using gas, DMSO, and ethanol solvents

σ*(C1-C5), yielding stabilization energies of 15.19 and 16.95 kJ/mol. These insights into the hyperconjugative and donor–acceptor interactions highlight the complex electronic structure of 1P3P2O, enhancing our understanding of its stability and reactivity.

Temperature-dependent effects

Temperature is a critical factor influencing chemical reactivity, thermodynamic properties, and pharmacodynamics, with a deep impact on the stability and behavior of compounds across varying temperature ranges. To explore the thermodynamic characteristics of the 1P3P2O molecule obtained using Density Functional Theory (DFT) methods with Perl scripts [55]. As shown in Table 6, the entropy values for 1P3P2O are 349.58 J/mol·K in the gas phase, 330.98 J/mol·K in DMSO, and 331.08 J/mol·K in ethanol. The heat capacity at 100 K for each solvent is recorded as 94.34 J/mol·K for the gas phase, 90.52 J/mol·K for DMSO, and 90.57 J/mol·K for ethanol, demonstrating an increase with rising temperature, as illustrated in Fig. S6. A comparison between DMSO and ethanol reveals a slight variation in their thermodynamic characteristics, indicating that both solvents exhibit similar properties.

Drug likeness and ADME prediction

In the realm of pharmaceutical research, evaluating the drug-likeness of a compound is a crucial step in determining its therapeutic potential. To assess the likelihood of a compound's effectiveness, several established criteria are used, including Lipinski's Rule of Five, the MDDR-like principle, Veber's rules, the Ghose filter, the CMC-50 standard, the blood–brain barrier (BBB) criterion, and the quantitative estimate of drug-likeness (QED) principle [56]. These criteria serve as indicators for determining how well a compound, like 1P3P2O, interacts with biological targets, particularly in inhibiting fungal growth. Key ADME (absorption, distribution, metabolism, and excretion) properties of 1P3P2O and its derivatives have been

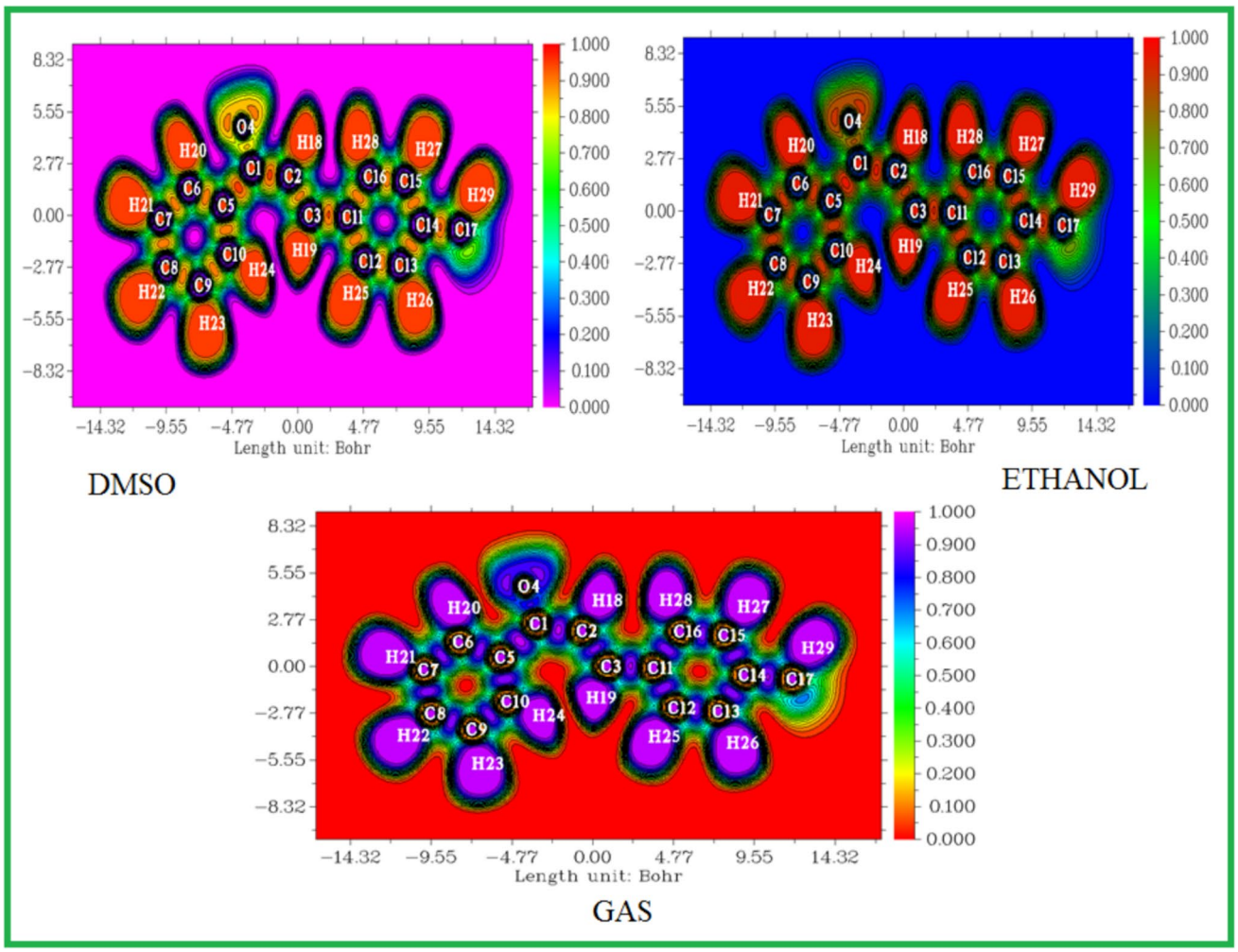

Fig. 8 LOL plot of title molecule using gas, DMSO, and ethanol solvents

Table 4 Dipole moment, polarizability, first-order hyperpolarizability (βtot) components of values

Parameters	GAS	DMSO	ETHANOL	Parameters	GAS	DMSO	ETHANOL
μx	0.4731	0.8590	1.0395	βxxx	− 1243.9653	− 4476.9028	− 6474.2892
μy	1.8400	1.4896	1.8093	βxxy	− 1076.6230	− 1798.9607	− 2711.8122
μz	0.0000	0.3081	0.3694	βxyy	− 638.4688	114.1267	157.9818
μ (D)	**1.8999**	**1.7469**	**2.1191**	βyyy	− 200.7521	− 7.1113	− 76.9787
axx	294.8453	367.9967	440.8961	βzxx	0.2078	− 321.3522	− 527.5580
axy	53.2371	0.0089	3.0325	βxyz	− 0.1599	1.4386	1.6475
ayy	222.5900	221.6784	273.1062	βzyy	− 0.1232	− 62.6077	− 23.8053
axz	− 0.0002	− 6. 5392	− 2.7421	βxzz	− 10.1992	29.5414	− 35.4847
ayz	− 0.0007	− 17.4908	− 11.5504	βyzz	48.3681	28.5902	60.3045
azz	94.7863	69.9124	150.2344	βzzz	− 0.0944	38.0770	28.9543
a (a.u)	204.0738	219.8625	288.0789	βtot (a.u)	2256.6611	4696.3816	6932.7348
Δa (a.u)	539.9910	687.6866	804.3853	**βtot (e.s.u)**	$\mathbf{19.5000 \times 10^{-30}}$	$\mathbf{4.0573 \times 10^{-30}}$	$\mathbf{5.9893 \times 10^{-30}}$
α_0 (e.s.u)	3.0243×10^{-23}	3.2583×10^{-23}	$4.2693 \times \mathbf{10^{-23}}$				
α (e.s.u)	$\mathbf{8.0026 \times 10^{-23}}$	$\mathbf{1.0191 \times 10^{-23}}$	$\mathbf{1.1921 \times 10^{-23}}$				

Table 5 Second order perturbation theory analysis of Fock matrix in NBO basis

Donor	Type	ED/e	Acceptor	Type	ED/e	[a] E(2) (Kj mol^{-1})	[b] E(j)-E(i) (a.u)	[c] F(I,J) (a.u)
C2-C3	σ	1.9713	C1-C2	σ*	0.0453	3.08	1.35	0.058
			C3-C11	σ*	0.0348	6.75	1.37	0.086
			C11-C12	σ*	0.0350	3.62	1.36	0.063
C3-C11	σ	1.9636	C2-C3	σ*	0.0186	5.75	1.37	0.08
			C11-C12	σ*	0.0350	6.64	1.36	0.085
			C11-C16	σ*	0.0407	6.85	1.36	0.086
C3-H19	σ	1.7809	C10-H24	σ*	0.1937	197.99	1.31	0.458
			C3-H19	σ*	0.2035	22.14	1.31	0.153
			C11-C16	σ*	0.0407	5.5	1.06	0.072
C5-C6	σ	1.9628	C1-C5	σ*	0.0636	6.68	1.34	0.085
			C5-C10	σ*	0.0311	8.16	1.38	0.095
			C6-C7	σ*	0.0190	4.26	1.39	0.069
C10-H24	σ	1.7742	C3-H19	σ*	0.2035	208.69	1.3	0.468
			C3-C11	σ*	0.0348	3.73	1.06	0.059
			C10-H24	σ*	0.1937	24.11	1.3	0.159
C11-C12	σ	1.9610	C3-C11	σ*	0.0348	7.01	1.37	0.088
			C11-C16	σ*	0.0407	7.39	1.36	0.09
			C12-C13	σ*	0.0197	5.53	1.38	0.078
C2-C3	π	1.7904	C1-O4	π*	0.2556	31.55	0.32	0.09
			C11-C12	π*	0.3972	18.68	0.32	0.073
			C5-C10	π*	0.3879	1.2	0.33	0.018
C1-O4	π	1.9290	C2-C3	π*	0.1518	9.49	0.4	0.056
			C5-C10	π*	0.3879	8.68	0.41	0.058
C6-C7	π	1.6383	C5-C10	π*	0.3879	22.67	0.31	0.075
			C8-C9	π*	0.3269	24.02	0.31	0.077
C8-C9	π	1.6446	C6-C7	π*	0.2902	19.63	0.32	0.072
			C5-C10	π*	0.3879	22.24	0.31	0.075
C11-C12	π	1.6058	C2-C3	π*	0.1518	23.48	0.31	0.081
			C13-C14	π*	0.3387	20.14	0.32	0.072
			C15-C16	π*	0.2851	21.03	0.31	0.074
C13-C14	π	1.6303	C11-C12	π*	0.3972	23.2	0.32	0.077
			C15-C16	π*	0.2851	19.38	0.31	0.071
C17-H30	σ	1.9787	C13-C14	π*	0.3387	3.17	0.55	0.041
			C14-C15	π*	0.0287	2	1.17	0.043
C17-H31	σ	1.9788	C13-C14	π*	0.3387	3.17	0.55	0.041
O4	LP(1)	1.9804	C1-C2	σ*	0.0453	1.47	1.3	0.039
			C1-C5	σ*	0.0636	1.51	1.29	0.04
O4	LP(2)	1.9210	C1-C2	σ*	0.0453	15.19	0.87	0.104
			C1-C5	σ*	0.0636	16.95	0.87	0.109
C1-O4	π*	0.2556	C6-C7	π*	0.2902	1.66	0.01	0.008
C13-C14	π*	0.3387	C17-H30	σ*	0.0081	1.66	0.32	0.049
			C17-H31	σ*	0.0081	1.66	0.32	0.049

[a] $E^{(2)}$ means energy of hyperconjugative interaction (stabilization energy)

[b] Energy difference between donor and acceptor i and j NBO orbitals

[c] F(i,j) is the Fock matrix element between i and j NBO orbitals

analyzed, with a focus on parameters viz., hydrogen bond acceptors (HBA), hydrogen bond donors (HBD), molar refractivity, skin permeability (log kp), topological polar surface area (TPSA), gastrointestinal absorption, BBB permeability, and bioavailability and the reported values are mentioned in Table 7. For a compound to be considered

Table 6 Thermodynamic properties at various temperatures

T(K)	Entropy S (J/mol K)			Heat capacity Cp (J/mol K)			Enthalpy H (kJ/mol)		
	Gas	**DMSO**	**Ethanol**	**Gas**	**DMSO**	**Ethanol**	**Gas**	**DMSO**	**Ethanol**
100	349.584	330.983	331.081	94.342	90.524	90.571	6.666	6.225	6.229
200	433.249	410.242	410.364	156.998	146.081	146.106	19.093	17.976	17.983
298.15	509.593	480.483	480.613	231.536	211.807	211.819	38.103	35.456	35.466
300	511.03	481.798	481.928	232.98	213.125	213.137	38.533	35.849	35.859
400	588.53	552.914	553.046	308.157	284.344	284.345	65.653	60.741	60.751
500	664.463	623.508	623.639	372.772	349.23	349.221	99.802	92.498	92.507
600	737.253	692.179	692.308	425.442	404.02	404.007	139.806	130.246	130.254
700	806.155	757.97	758.097	468.152	449.292	449.277	184.558	172.984	172.991
800	871.03	820.49	820.614	503.203	486.799	486.784	233.181	219.845	219.851
900	932.034	879.692	879.814	532.375	518.185	518.171	285.003	270.14	270.144
1000	989.432	935.699	935.82	556.935	544.714	544.702	339.503	323.321	323.324

Table 7 Drug likeness parameters of 1P3P2O

Descriptors	Values
Num. H-bond acceptors(HBA)	1
Num. H-bond donors (HBD)	0
Molar Refractivity	71.21
TPSA	17.07 $Å^2$
Lipinski	Yes; 0 violation
Bioavailability Score	0.55
miLogP	4.26

drug-like, it should exhibit HBD and HBA values under 10, a TPSA value below 140, and a molar refractivity between 40 and 130. The values for 1P3P2O fall within these ideal ranges, indicating its potential as a promising pharmaceutical candidate. Additionally, 1P3P2O shows favorable characteristics in terms of skin permeability, gastrointestinal absorption, BBB penetration, and bioavailability when compared to known antifungal agents. This makes it a strong candidate for further investigation as a pharmaceutical lead. A comparison with existing derivatives reveals that 1P3P2O not only meets the drug-likeness criteria but also demonstrates significant antifungal and antiviral activity. This highlights its potential as an effective treatment, advancing its role in the development of novel antifungal therapies and driving further research in pharmaceutical applications.

Analysis of Hirshfeld surfaces and energy frameworks

The intramolecular interactions of 1P3P2O molecule are evaluated using Hirshfeld Surface Analysis (HAS) as shown in Figs. S7(A-E). The parameter values include: Dnorm: – 0.1599 to – 1.3286, di: 1.0319 to 2.5537 Å, de: 1.0328 to 2.5529 Å, shape index: – 0.9774 to 0.977, and curvedness: – 3.8896 to 0.1674. Color-coded surfaces are indicated, with red for short-range contacts, blue for long-range interactions, and white for van der Waals separations to explain the molecular interactions. Figure 9 shows a 2D fingerprint analysis to investigate these interactions. The crystal's primary intermolecular interactions were H–H (50%), O–H/H–O (14.7%), H-C/C-H (30.8%), O-C/C- (0.6%), and C–C (3.4%). These results match the Hirshfeld surface's donor–acceptor zones, validating the single crystal report [17]. Crystal stabilization energy, including electrostatic and dispersion energies, was also examined. Figure 9 shows these energies as blue and green cylinders. The dispersion energy is crucial for stabilizing the structure, as seen in Fig. S8(a) with the interaction of the yellow 1P3P2O molecule and its neighbors within a 3.8 Å radius. Fig. S8(b) shows energy contributions in red, green, and blue cylinders for electrostatic, dispersion, and total energies. This research shows that dispersion interactions dominate 1P3P2O Chalcone crystal structure stabilization.

Molecular docking

Molecular docking illustrates the biological potential of the investigated molecule and explains how small molecules interact with protein targets [57, 58, 59]. In this study, the antiviral and antifungal activity of 1P3P2O is investigated, and 6W97 (inflammation) and 2RFX (antiviral) proteins are obtained from the Protein Data Bank. We assessed the biological activity of the 1P3P2O molecule using the Passonline server [60]. The number of interacting residues, bond lengths, and docking energies (in kcal/mol) are summarized in Table 8. The 3D and 2D protein–ligand (6W97 and 2RFX) interactions are displayed in Figs. 10 and 11. The 6W97 receptor is observed to have

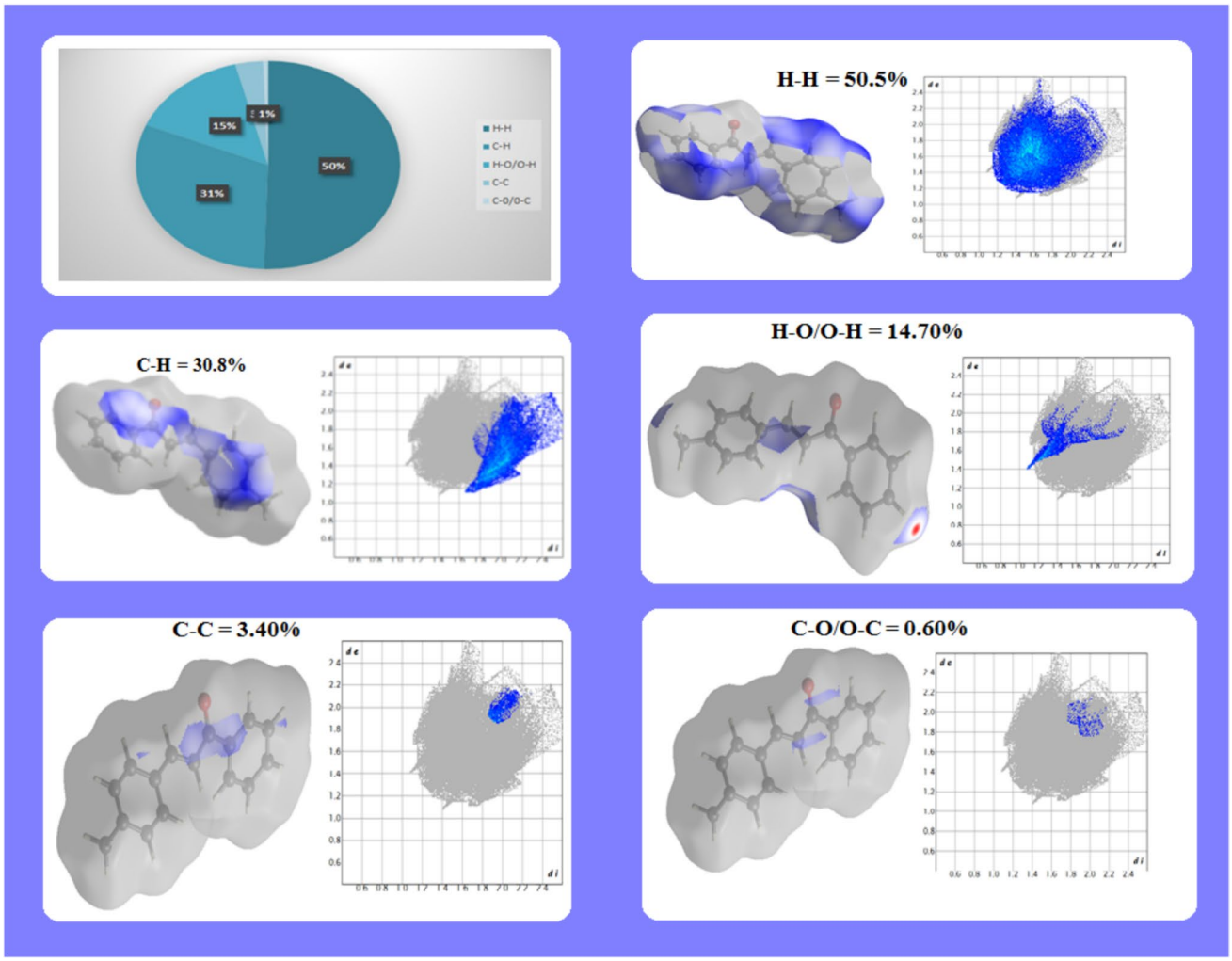

Fig. 9 2D-Finger print plot of 1P3P2O molecule

Table 8 Molecular docking with ligand and 4ZRT target protein

Protein (PDB ID)	Bonded residues	No. of hydrogen bond	Bond distance	Estimated inhibition constant (μm)	Binding energy (kcal/mol)	Intermolecular energy (kcal/mol)	Reference RMSD(Å)
6W9L	LEU A:9 GLY A:8	2	1.88 2.8	84.66	− 7.56	− 5.81	70.96
2RFX	TYR A:68 LYS A:125	2	3.13 3.14	163.72	− 7.17	− 5.36	55.527

the least binding energy of the 1P3P2O molecule at − 7.56 kcal/mol. In contrast, the interaction with 2RFX results in a slightly higher binding energy of − 7.17 kcal/mol. Overall, the lowest binding energies suggest the 1P3P2O molecule has promising antiviral and anti-inflammatory activities.

Conclusion

The chalcone derivative of the 1P3P2O molecule is successfully synthesized and characterized using FT-IR, NMR, and UV–Vis spectroscopic techniques. The most stable structure of the 1P3P2O molecule was identified using

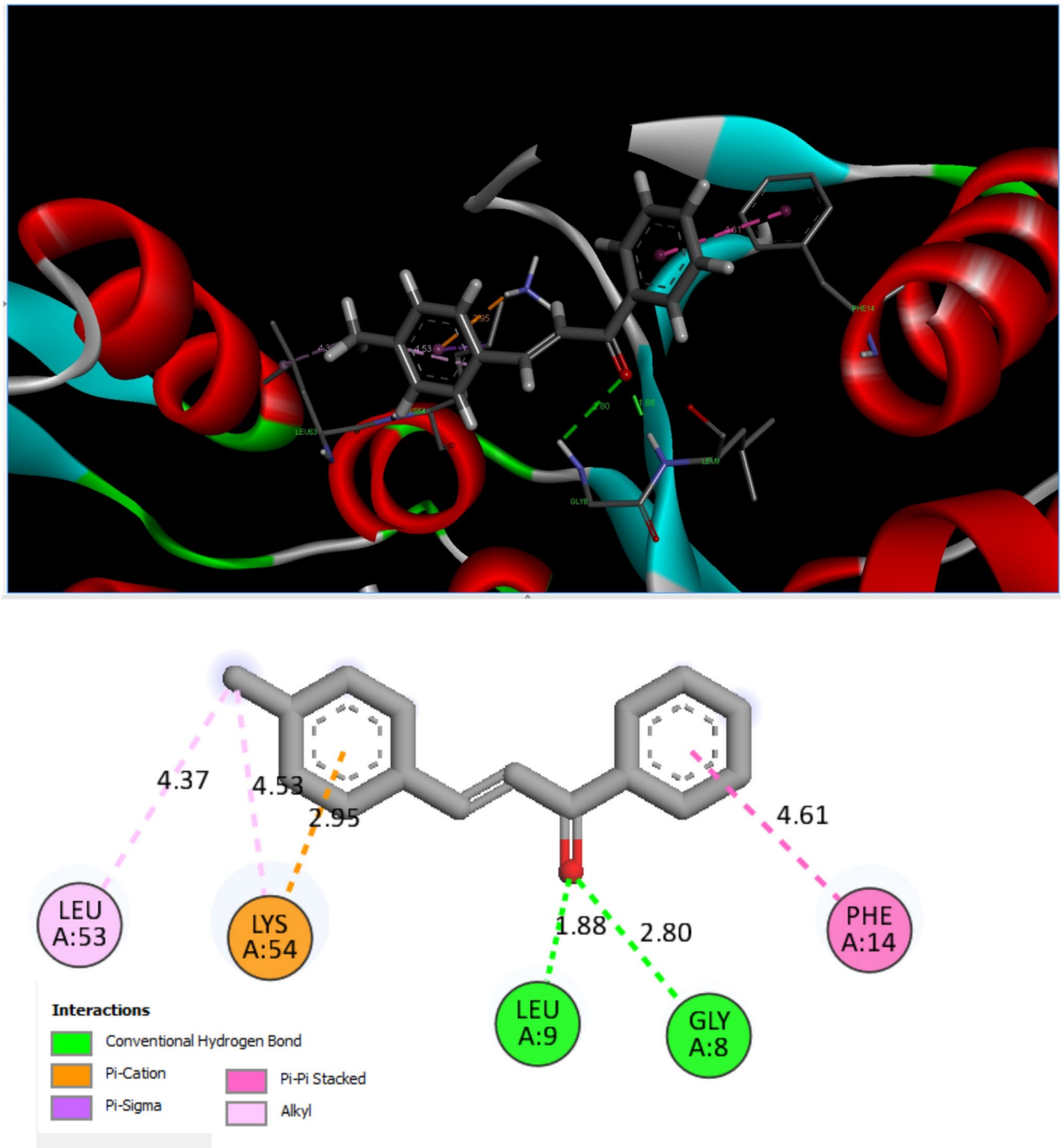

Fig. 10 3D and 2D molecular docking diagram of title molecule with 6W9L protein

PES analyses. This stable molecular structure is applied to calculate the entire theoretical investigation. The energy transition was evaluated in different phases (gas, DMSO, and ethanol) for ground to first excited states using UV–Vis and HOMO–LUMO analyses. The least band gap energy is observed at 3.6 to 4.0 eV. The chemical reactivity of the title molecule is evaluated using MEP and Fukui function analyses; both studies provide well-consistent results of electrophilic and nucleophilic natures. Particularly, the O4 atom is observed to have negative potential with the 1P3P2O molecule. The Natural Bond Orbital (NBO) analysis reveals the highest stabilization energy related to the interaction between LP2(O4) with σ*(C1-C2) and σ*(C1-C5) bonds, which contributes significantly to the compound's unique

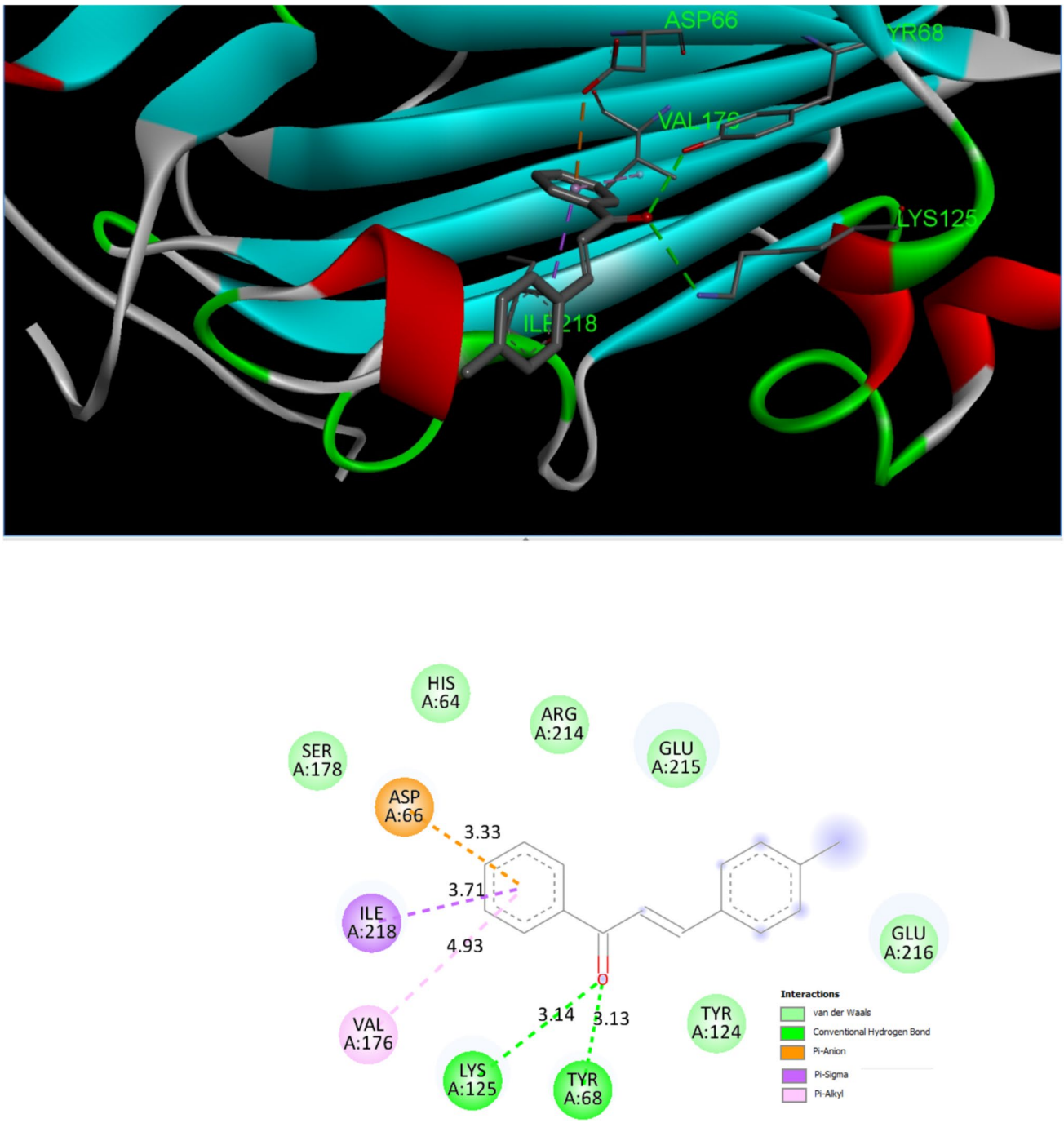

Fig. 11 3D and 2D molecular docking diagram of title molecule with 2RFX protein

properties. Nonlinear optical (NLO) properties were also examined, and the first-order hyperpolarizability of the title molecule is nine times more than the standard material of urea. The thermal stability of 1P3P2O was evaluated at various temperatures through DFT, providing a clearer picture of its chemical stability under different conditions. In the pharmaceutical context, the compound was assessed for drug-likeness and ADMET parameters. The antiviral and antifungal activity of the 1P3P2O molecule is investigated using molecular docking investigations. The strong binding interaction is observed with antiviral protein 6W9L, with the least binding energy of − 7.56 kcal/mol.

Supplementary Information The online version contains supplementary material available at https://doi.org/10.1007/s11224-025-02600-9.

Author contributions Mohamed Ibrahim Sulaiman Sait Shahul Hameed—Conceptualization, Methodology, Validation, Formal analysis, Writing Original Draft, Writing- Review, Visualization Raj Muhamed Rahiman Sahib—Investigation, Supervision, Project administration, Writing- Editing Kumaran Subramanian—Formal analysis, Validation, Writing, Methodology, Investigation Muzammil Pookutti—Investigation, Visualization, Methodology Thirunavukkarasu Manickavelu—Validation, Formal analysis, Writing- Review, Visualization Naveen Kosar—Investigation, Visualization, Writing- Editing Rajesh Punniyamoorthy—Validation, Writing, Methodology, Investigation Chakkaravarthy Perumal—Validation, Formal analysis, Writing-Review, Visualization Dhanalakshmi Karuppaiyan—Investigation, Formal analysis, Writing- Review, Visualization Raja Murugesan—Conceptualization, Resources, Investigation, Review, Writing- Editing.

Data availability No datasets were generated or analysed during the current study.

Declarations

Ethics approval Not applicable.

Competing interests The authors declare no competing interests.

References

1. Takaki R (2022) Ashburn BO (2022) (E)-3-[4-(1 H-Imidazol-1-yl) phenyl]-1-(3-chloro-4-fluorophenyl) prop-2-en-1-one. Molbank 2:1–4. https://doi.org/10.3390/M1375
2. Bailey N (2021) Ashburn BO (2021) (E)-3-[4-(1 H-Imidazol-1-yl) phenyl]-1-(4-methylphenyl) prop-2-en-1-one. Molbank 3:1–4. https://doi.org/10.3390/M1269
3. Koh D (2022) (E)-1-(2-Hydroxy-4, 6-dimethoxyphenyl)-3-(naphthalen-1-yl) prop-2-en-1-one. IUCrData 72021(9):x220932
4. Rasool F, Hussain A, Ayub K, Tariq M, Mahmood K, Yousuf S (2022) Yar M (2022) Experimental and Theoretical investigations on (E)-3-(4-ethoxyphenyl)-1-(2-(trifluoromethyl) phenyl) prop-2-en-1-one and (E)-3-(naphthalen-2-yl)-1-(2-(trifluoromethyl) phenyl) prop-2-en-1-one: DNA binding, Urease inhibition and Promising NLO response. J of Mol Struc 1253:132194
5. Aldaghri O (2021) Spectral characteristics and molecular structure of (E)-1-(4-Chlorophenyl)-3-(4-(Dimethylamino) Phenyl) Prop-2-en-1-One (DAP). Materials 14(11):2766
6. Zou WS, Jiang LW, Jia S, Zhu WF (2017) (E)-3-(dimethylamino)-1-(1H-indol-3-yl) prop-2-en-1-one. In: 2017 2nd International Conference on Biological Sciences and Technology (BST 2017) 2018(6):251–254
7. Sadgir NV, Dhonnar SL, Jagdale BS, Sawant AB (2022) Synthesis, spectroscopic characterization, XRD crystal structure, DFT and antimicrobial study of (2E)-3-(2, 6-dichlorophenyl)-1-(4-methoxyphenyl)-prop-2-en-1-one (2022) SN. Appl Sci 2020(2):1–12
8. Borul SB (2020) Agarkar SV (2020) Synthesis and study of drug likeness property of (E)-3-substituted phenyl-1-Piperidino-2-Propen-1-one Cinnamamide. Journal of Emerging Technologies and Innovative Research (JETIR) 7(3):46–50
9. Medimagh M, Issaoui N, Gatfaoui S, Al-Dossary O, Kazachenko AS, Marouani H (2021) Wojcik MJ (2021) Molecular modeling and biological activity analysis of new organic-inorganic hybrid: 2-(3,4-dihydroxyphenyl) ethanaminium nitrate. Journal of King Saud University - Science 33(8):101616
10. Jumabaev A, Holikulov U, Hushvaktov H (2023) ISSAOUI N, Absanov A (2023) Intermolecular interactions in ethanol solution of OABA: Raman, FTIR, DFT, M062X, MEP, NBO, FMO, AIM, NCI, RDG analysis. J Mol Liq 377:121552
11. Noureddine O, Issaoui N, Gatfaoui S, Al-Dossary O (2021) Marouani H (2021) Quantum chemical calculations, spectroscopic properties and molecular docking studies of a novel piperazine derivative. Journal of King Saud University - Science 33(2):101283
12. Habli H, Mejrissi L, Issaoui N, Yaghmour SJ, Oujia B, Gadéa FX (2015) Ab initio calculation of the electronic structure of the strontium hydride ion (SrH+). Int J Quantum Chem 115(3):172–186
13. Kazachenko AS, Medimagh M, Issaoui N, Al-Dossary O, Wojcik MJ, Kazachenko AS, Miroshnokova AV (2022) Malyar YN (2022) Sulfamic acid/water complexes (SAA-H2O(1–8)) intermolecular hydrogen bond interactions: FTIR, X-ray, DFT and AIM analysis. J Mol Struct 1265:133394
14. Frisch MJ, Trucks GW, Schlegel HB, Scuseria GE, Ortiz JV, Cioslowski J, Fox DJc (2009) Gaussian 09, Revision E.01 Gaussian, Inc. Wallingford CT
15. Lu T (2012) Chen F (2012) Multiwfn: a multifunctional wavefunction analyzer. J Comput Chem 33(5):580–592. https://doi.org/10.1002/jcc.22885
16. Morris GM, Huey R, Lindstrom W, Sanner MF, Belew RK, Goodsell DS, Olson AJ (2009) Autodock4 and AutoDockTools4: automated docking with selective receptor flexiblity. J Comput Chem 30(16):2785–91
17. Edward M (2006) Treadwell 4-Methylchalcone Department of Chemistry. Eastern Illinois University, 600 Lincoln Avenue, Charleston, IL 61920, USA
18. Raja M, Raj Muhamed R, Muthu S (2017) Suresh M (2017) Synthesis, spectroscopic (FT-IR, FT-Raman, NMR, UV–Visible), NLO, NBO, HOMO-LUMO, Fukui function and molecular docking study of (E)-1-(5-bromo-2-hydroxybenzylidene)semicarbazide. J Mol Struct 1141:284–298
19. Janani S, Hemamalini R, Muthu S, Aayisha S (2021) Raja M (2021) Molecular structure, spectroscopic (FT-IR, FT-Raman, NMR), HOMO-LUMO, chemical reactivity, AIM, ELF, LOL and Molecular docking studies on 1-Benzyl-4-(N-Boc-amino) piperidine. J Mol Struct 1230:129657
20. Swarnalatha N, Gunasekaran S, Muthu S (2015) Nagarajan M (2015) Molecular structure analysis and spectroscopic characterization of 9-methoxy-2H-furo[3,2-g]chromen-2-one with experimental (FT-IR and FT-Raman) techniques and quantum chemical calculations. Spectrochim Acta part A 137:721–729
21. Wade LG (1992) Advanced Organic Chemistry, 4th edn. Wiley, New York, p 723
22. Mathew V, Keshavayya J (2007) Vaidya VP (2007) Synthesis, characterization and pharmacological activities of 3, 6-disubstituted-1, 2, 4-triazolo [3, 4-b]-1, 3, 4-thiadiazoles and their dihydro analogues. E-J Chem 4:320–342
23. Koczon P (2003) Dobrowolski JCz, Lewandowski W (2003) Mazurek AP, Experimental and theoretical IR and Raman spectra of picolinic, nicotinic and isonicotinic acids. J Mol Struct 655:89–95
24. Raja M, Raj Muhamed R, Muthu S (2017) Suresh M (2017) Synthesis, spectroscopic (FT-IR, FT-Raman, NMR, UV–Visible), first order hyperpolarizability, NBO and molecular docking study of (E)-1-(4-bromobenzylidene)semicarbazide. J Mol Struct 1128:481–492
25. Cherif A (2023) Importance of solvents role in molecular and electronic properties, DFT, spectroscopic, electron-hole transition, chemical reactivity, topology and molecular docking

investigations of (±)-2-(2-{4-[(4-chlorophenyl)-phenylmethyl] piperazin-1-yl} ethoxy)ethanol. J Mol Liq 2023(391):123278
26. Jamróz MH, Dobrowolski JCz, Brzozowski R (2006) Vibrational modes of 2,6-, 2,7-, and 2,3-diiso-propylnaphthalene. A DFT study. J Mol Struct (787):172–183
27. Krishnakumar V, Balachandran V (2005) Chithambarathanu T (2005) Density functional theory study of the FT-IR spectra of phthalimide and N-bromophthalimide. Spectrochim Acta Part A Mol Biomol Spectrosc 62(4–5):918–925
28. Jumabaev A, Holikulov U, Hushvaktov H, ISSAOUI N, Absanov A (2023) Intermolecular interactions in ethanol solution of OABA: Raman, FTIR, DFT, M062X, MEP, NBO, FMO, AIM, NCI, RDG analysis. J Mole Liq 377:121552
29. Sharma D (2016) Tiwari SN (2016) Comparative computational analysis of electronic structure, MEP surface and vibrational assignments of a nematic liquid crystal: 4-n-methyl-4´-cyanobiphenyl. J Mol Liq 214:128–135
30. Daghar C, Issaoui N, Roisnel T, Dorcet V, Marouani H (2021) Empirical and computational studies on newly synthesis cyclohexylammonium perchlorate. J Mol Struct 2021(1230):129820
31. Bibi N, Kosar N, Ayub K (2020) Mahmood T (2020) Theoretical investigation on radical anion promoted electrocyclization in photochromes. J Mol Graph Model 97:107550
32. Dege N, Gökce H, Doğan OE, Alpaslan G, Ağar T, Muthu S (2022) Sert Y (2022) Quantum computational, spectroscopic investigations on N-(2-((2-chloro-4,5-dicyanophenyl)amino) ethyl)-4-methylbenzenesulfonamide by DFT/TD-DFT with different solvents, molecular docking and drug-likeness researches. Colloids Surf, A 638:128311
33. Avcı D, Altürk S, Sönmez F, Tamer O, Başoğlu A, Atalay Y, Zengin Kurt B, Öztürk D (2019) Dege N (2019) A new dinuclear copper (II) complex of 2,5–Furandicarboxylic acid with 4(5)-Methylimidazole as a high potential α-glucosidase inhibitor: synthesis, crystal structure, cytotoxicity study, and TD/DFT calculations. Appl Organomet Chem 33(3):e4725
34. Gatfaoui S, Issaoui N, Roisnel T (2021) Marouani H (2021) Synthesis, experimental and computational study of a non-centrosymmetric material 3-methylbenzylammonium trioxonitrate. J Mol Struct 1225:129132
35. Guerroudj AR, Boukabcha N, Benmohammed A, Dege N, Houda Belkafouf NE, Khelloul N, Djafri A, Chouaih A (2012) Synthesis, crystal structure, vibrational spectral investigation, intermolecular interactions, chemical reactivity, NLO properties and molecular docking analysis on (E)-N-(4-nitrobenzylidene)-3-chlorobenzenamine: A combined experimental and theoretical study. J of Mol Struc 2012(1240):130589
36. Demirtaş G, Dege N, İçbudak H, Yurdakul O (2012) Büyükgüngör O (2012) Experimental and DFT Studies on Poly[di-μ3-acesulfamato-O,O:O′;O′:O,O-di-μ-acesulfamato-O,O; N-di-μ-aqua-dicalcium(II)] Complex. J Inorg Organomet Polym Mater 22:671–679
37. Kansız S (2018) Dege N (2018) Synthesis, crystallographic structure, DFT calculations and Hirshfeld surface analysis of a fumarate bridged Co (II) coordination polymer. J of Mol Struct 1173:42–51
38. Rajkumar K, Gokulakrishnan V, Anand S (2024) Durga R (2024) Spectroscopic, quantum computational, topological, Fukui functions and molecular docking analysis on a potential anti-cancer molecule nicotinamide by DFT method. J Mol Struct 1300:137216
39. Zamora PP, Bieger K, Cuchillo A, Tello A, Muena JP (2021) Theoretical determination of a reaction intermediate: Fukui function analysis, dual reactivity descriptor and activation energy. J Mol Struct 1227:129369
40. Khemalapure SS, Katti VS, Hiremath CS, Hiremath SM, Basanagouda M (2019) Radder SB (2019) Spectroscopic (FT-IR, FT-Raman, NMR and UV-Vis), ELF, LOL, NBO, and Fukui function investigations on (5-bromo-benzofuran-3-yl)-acetic acid hydrazide (5BBAH): experimental and theoretical approach. J Mol Struct 1196:280–290
41. Wang T, Weerasinghe KC (2017) Sun HLi, Liu, Li W, Hu W, Zhou X, Wang L, (2017) Characterization of photo-induced electron and hole transfer in a porphyrin based ambipolar organic molecule with cascade energy levels. J Mol Struct 1142:226–238
42. Rajmohan V, Deepa S, Asha S, Priya SV (2023) Abir Sagaama, Raja M (2023) Synthesis, solvation effects, spectroscopic, chemical reactivity, topological analysis and biological evaluation of 4-chloro-N-(2, 6-dichlorobenzylidene) benzohydrazide. J Mol Liq 390:122955
43. Hammami F, Issaoui N (2021) Nasr S (2021) Investigation of hydrogen bonded structure of urea-water mixtures through infrared spectroscopy and non-covalent interaction (NCI) theoretical approach. Comput Theor Chem 1199:113218
44. Bhattacharya S, Biswas C, Sai Santosh Kumar R, Jonnadula Venkata Suman K, Narra Vamsi K, Lingamallu G, Venugopal RS (2019) Synthesis, optical, electrochemical, DFT studies, NLO properties, and ultrafast excited state dynamics of carbazole-induced phthalocyanine derivatives. J Phys Chem C12(17):11118–11133
45. Irshad S, Ullah F, Khan S, Ludwig R (2021) Tariq Mahmood, Ayub K (2021) First row transition metals decorated boron phosphide nanoclusters as nonlinear optical materials with high thermodynamic stability and enhanced electronic properties; A detailed quantum chemical study. Opt Laser Technol 134:106570
46. Ullah F, Kosar N, Ali A (2020) Maria, Tariq Mahmood, Khurshid Ayub (2020) Design of novel inorganic alkaline earth metal doped aluminum nitride complexes (AEM@Al12N12) with high chemical stability, improved electronic properties and large nonlinear optical response. Optik 207:163792
47. Rasul R, Mahmood T, Ayub K (2023) Khurram Saleem Joya, Farooq Anwar, Nazamid Saari, Nawaz R, Mazhar Amjad Gilani (2023) Alkali metals doped cycloparaphenylene nanohoops: promising nonlinear optical materials with enhanced performance. Heliyon 9:e21508
48. Buvaneswari PR (2024) Simon Jeya Sunder Raj M, Sudha K, Aravind T, Chakkaravarthy P, Raja M (2024) Comprehensive analysis of (E)-3-(4-chlorophenyl)-1-(4-methoxyphenyl)prop-2-en-1-one (4CP4MPO): synthesis, spectroscopic, salvation electronic properties, electron-hole transition, topological, Hirshfeld surface and molecular docking analysis. Chemical Physics Impact 8:100452
49. Habib Rahuman M, Muthu S, Raajaraman BR (2020) Raja M (2020) Quantum computational, spectroscopic and molecular docking investigations on 4-Acetylamino-benzoic acid methyl ester: a prospective anticancer drug. Chemical Data Collections 26:100352
50. Rajasekar R, Renuga Devi TS, Janani S, Raja M (2023) Sunil Kumar, Ramesh P, Muthu S, Saleem Javed (2023) Molecular structure, physicochemical properties, impact of solvents ionization potential, electron occupancy, inhibition constant, and stabilization energy investigations of 4-acetamido benzoic acid. Chemical Physics Impact 7:100328
51. Scott AP, Radom L (1996) Harmonic vibrational frequencies: an evaluation of Hartree-Fock, Moller-Plesset, quadratic configuration interaction, density functional theory, and semiempirical scale factors. J Phys Chem 100:16502–16513
52. Sangeetha P, Mullainathan S, Rajasekaran L, Muthu S (2021) Ahmad Irfan, Saral A (2021) Electronic properties of solvents (Water, Benzene, Ethanol) using IEFPCM model, spectroscopic exploration with drug likeness and assessment of molecular docking on 1-Octanesulfonic Acid Sodium Salt. J Mol Liq 344:117719
53. Balakrishnan PD, Rath NP, Premkumar T, Ganesh A (2023) Kanchana P (2023) Facile and green synthesis, crystal structure, antibacterial activity, Hirshfeld surface analysis, and computational

investigation of a novel lithium(I) complex: comparisons of theoretical and experimental analyses. J Mol Liq 391:123118
54. Mhadhbi N, Issaoui N (2022) Hamadou WS, Alam JM, Elhadi AS, Mohd Adnan, Houcine Naïli, Riadh Badraoui (2022) Physicochemical properties, pharmacokinetics, molecular docking and in-vitro pharmacological study of a cobalt (II) complex based on 2-aminopyridine. ChemistrySelect 7(3):e202103592
55. Medimagh M (2023) Cherifa Ben Mleh, Noureddine ISSAOUI, Kazachenko AS, Thierry Roisnel, Al-Dossary OM, Houda Marouani, Bousiakoug LG (2023) DFT and molecular docking study of the effect of a green solvent (water and DMSO) on the structure, MEP, and FMOs of the 1-ethylpiperazine-1,4-diium bis(hydrogenoxalate) compound. J Mol Liq 369:120851
56. Lefi N, Kazachenko AS, Raja M, Issaoui N (2023) Kazachenko AS (2023) Molecular structure, spectral analysis, molecular docking and physicochemical studies of 3-bromo-2-hydroxypyridine monomer and dimer as bromodomain inhibitors. Molecules 28:2669
57. Santhy KR, Daniel Sweetlin M, Muthu S, Raja M (2019) Christina Susan Abraham (2019) Optical, vibrational (FT-IR and FT-Raman), electronic and molecular docking investigations of 1 Phenyl Isatin. Optik 182:1211–1227
58. Al-Rabiah H, Muthu S, Al-Omary FAM, Al-Tamimi AMS, Raja M, Raj Muhamed R (2017) El-Emam AA (2017) Molecular structure, vibrational spectra, NBO, Fukui function, homo-lumo analysis and molecular docking study of 6-[(2-methylphenyl) sulfanyl]-5-propylpyrimidine-2,4(1h,3h)-dione. Maced J Chem Chem Eng 36:59–80
59. Buvaneswari PR (2024) Simon Jeya Sunder Raj M, Sudha M, Aravind T, Chakkaravarthy P, Raja M (2024) Comprehensive analysis of (E)-3-(4-chlorophenyl)-1-(4-methoxyphenyl) prop-2-en-1-one (4CP4MPO): synthesis, spectroscopic, salvation electronic properties, electron-hole transition, topological, Hirshfeld surface and molecular docking analysis. Chemical Physics Impact 8:100452
60. Filimonov DA, Lagunin AA, Gloriozova TA, Rudik AV, Druzhilovskii DS, Pogodin PV (2014) Poroikov VV (2014) Prediction of the biological activity spectra of organic compounds using the PASS online web resource. Chem Heterocycl Compd 50(3):444–457